Draft version September 30, 2020
Typeset using LaTeX **twocolumn** style in AASTeX62

The progenitor of the supernova imposter AT 2019krl: a SN 2008S-like transient from a blue supergiant

Jennifer E. Andrews,[1] Jacob E. Jencson,[1] Schuyler D. Van Dyk,[2] Jack M. M. Neustadt,[3] Nathan Smith,[1] David J. Sand,[1] K. Kreckel,[4] C.S. Kochanek,[3] S. Valenti,[5] Jay Strader,[6] M.C. Bersten,[7,8,9] Guillermo A. Blanc,[10,11] K. Azalee Bostroem,[5] Thomas G. Brink,[12] Eric Emsellem,[13,14] Alexei V. Filippenko,[12,15] Gastón Folatelli,[7,8,9] Mansi M. Kasliwal,[16] Frank J. Masci,[2] Rebecca McElroy,[17] Dan Milisavljevic,[18] Francesco Santoro,[19] and Tamás Szalai[20,21]

[1] *Steward Observatory, University of Arizona, 933 North Cherry Avenue, Tucson, AZ 85721-0065, USA*
[2] *Caltech/Spitzer Science Center, Caltech/IPAC, Mailcode 100-22, Pasadena, CA 91125, USA*
[3] *Department of Astronomy, The Ohio State University, 140 West 18th Avenue, Columbus, OH 43210, USA*
[4] *Astronomisches Rechen-Institut, Zentrum für Astronomie der Universität Heidelberg, Mönchhofstraße 12-14, 69120 Heidelberg, Germany*
[5] *Department of Physics, University of California, 1 Shields Avenue, Davis, CA 95616-5270, USA*
[6] *Department of Physics and Astronomy, Michigan State University, East Lansing, MI 48824, USA*
[7] *Instituto de Astrofísica de La Plata (IALP), CONICET, Paseo del bosque S/N, 1900, Argentina*
[8] *Facultad de Ciencias Astronómicas y Geofísicas, Universidad Nacional de La Plata, Paseo del Bosque, La Plata, Argentina*
[9] *Kavli Institute for the Physics and Mathematics of the Universe (WPI), The University of Tokyo, 5-1-5 Kashiwanoha, Kashiwa, Chiba, Japan*
[10] *The Observatories of the Carnegie Institution for Science, 813 Santa Barbara Street, Pasadena, CA 91101, USA*
[11] *Departamento de Astronomía, Universidad de Chile, Casilla 36-D, Santiago, Chile*
[12] *Department of Astronomy, University of California, Berkeley, CA 94720-3411, USA.*
[13] *European Southern Observatory, Karl-Schwarzschild-Straße 2, D-85748 Garching bei München, Germany*
[14] *Univ. Lyon, ENS de Lyon, CNRS, Centre de Recherche Astrophysique de Lyon UMR5574, F-69230 Saint-Genis-Laval France*
[15] *Miller Senior Fellow, Miller Institute for Basic Research in Science, University of California, Berkeley, CA 94720 USA*
[16] *Division of Physics, Mathematics, and Astronomy, California Institute of Technology, Pasadena, CA 91125, USA*
[17] *Sydney Institute for Astronomy, School of Physics, A28, The University of Sydney, NSW, 2006, Australia*
[18] *Department of Physics and Astronomy, Purdue University, 525 Northwestern Avenue, West Lafayette, IN 47907, USA*
[19] *Max Planck Institut für Astronomie, Königstuhl 17, D-69117 Heidelberg, Germany*
[20] *Department of Optics and Quantum Electronics, University of Szeged, H-6720 Szeged, Dóm tér 9., Hungary*
[21] *Konkoly Observatory, Research Centre for Astronomy and Earth Sciences, H-1121 Budapest, Konkoly Thege Miklós út 15-17, Hungary*

(Received September 30, 2020; Revised September 30, 2020; Accepted September 30, 2020)

Submitted to ApJ

ABSTRACT

For a recent intermediate-luminosity transient, AT 2019krl in M74 (NGC 628) at a distance of only ~ 9.8 Mpc, extensive archival *Hubble Space Telescope (HST)*, *Spitzer Space Telescope*, and Large Binocular Telescope (LBT) imaging reveal a bright optical and mid-infrared progenitor star. While the optical peak of the event was missed, a peak was detected in the infrared with an absolute magnitude of $M_{4.5\,\mu\mathrm{m}} = -18.4$ mag, leading us to infer a visual-wavelength peak absolute magnitude of -13.5 to -14.5. The light curve from the pre-discovery archival data indicated no outbursts over the previous 16 yr. The colors, magnitudes, and inferred temperatures of the progenitor best match a 13–14 $M_\odot$ yellow or blue supergiant, if only foreground extinction is taken into account, or a hotter and more massive star, if any additional local extinction is included. A pre-eruption spectrum of the star reveals strong Hα emission having a narrow line core with a width of about 200 km s^{-1} (FWHM) and with wings extending to $\pm$ 2000 km s^{-1}. The post-eruption spectrum is fairly flat and featureless with only Hα, Na I D, [Ca II], and the Ca II near-infrared triplet in emission, with very little change in the shape of Hα over 120 days. As in many previous intermediate-luminosity transients, AT 2019krl

Corresponding author: Jennifer E. Andrews
jandrews@as.arizona.edu

shows remarkable similarities to both massive luminous blue variable (LBV) eruptions and SN 2008S-like events. However, in this case, the information about the pre-eruption star allows us to clearly rule out both a super-AGB star and an electron-capture SN as the origin of this SN 2008S-like event. Instead, the data favor either a relatively unobscured blue supergiant (likely viewed pole-on) or a highly extinguished LBV with $M > 20$ M$_\odot$, confirming that BSGs or LBVs that may undergo mergers are a viable progenitor pathway to produce SN 2008S-like events.

Keywords: stars: massive, supergiants — supernovae: individual (AT 2019krl)

1. INTRODUCTION

Existing in the magnitude space between traditional supernovae (SNe) and classical novae lies a menagerie of explosive and eruptive transients with peak magnitudes in the range $-10 < M_V < -15$ mag and optical spectra dominated by narrow- or intermediate-width Balmer emission lines. These "SN imposters" (Van Dyk et al. 2000; Smith et al. 2011; Kochanek et al. 2012; Van Dyk & Matheson 2012) may arise from a variety of progenitors and have been attributed to a number of potential physical mechanisms, including instabilities near the Eddington limit (Smith & Owocki 2006; Owocki et al. 2004), instabilities in nuclear burning in late post-main-sequence evolution (Shiode & Quataert 2014; Smith & Arnett 2014), stellar mergers or common-envelope phases in binary star systems (Soker & Kashi 2013; Kochanek et al. 2014; Smith et al. 2016b, 2018), or electron-capture supernovae (ecSNe; Botticella et al. 2009; Kochanek et al. 2012; Adams et al. 2016).

Originally, the handful of known SN imposters were interpreted as giant eruptions of luminous blue variables (LBVs) akin to η Carinae's Great Eruption (Humphreys et al. 1999). Over the years, as more intermediate-luminosity transients have been discovered and a broader diversity was seen in their light curves, spectra, and possible progenitors, they were grouped into three broad classes of events: giant eruptions of LBVs in massive stars, SN 2008S-like events (also known as intermediate-luminosity red transients, ILRTs, or intermediate-luminosity optical transients, ILOTs) that have been proposed as eruptions of blue supergiants or explosions of super-asymptotic giant branch (AGB) stars as ecSNe, and luminous red novae (LRNe), which have usually been interpreted as binary mergers or common-envelope (CE) ejections in low- or intermediate-mass stars. All of these involve large amounts of episodic mass loss, and many of them share observed properties that blur the distinction between categories. For example, LBVs can experience super-Eddington eruptions which are accompanied by large amounts of mass loss (Smith & Owocki 2006; Owocki et al. 2004), but some LBV eruptions might also be the result of stellar mergers (Smith et al. 2016b, 2018). The most well known example of the phenomenon was the Great Eruption of η Car (Smith 2012; Smith et al. 2018). The SN 2008S-like events are characterized by a highly obscured dusty progenitor, and strong [Ca II] and Ca II near-infrared (NIR) triplet emission lines in their spectra (Prieto et al. 2008, 2009; Thompson et al. 2009), but some LBVs including η Car exhibit all these properties as well (Smith et al. 2011, 2016b, 2018). The SN2008S-like transients have been interpreted as arising either from a terminal low-luminosity SN event (Botticella et al. 2009; Kochanek et al. 2012; Adams et al. 2016) or from massive-star outbursts in a dusty cocoon (Berger et al. 2009; Smith et al. 2009).

With the discovery that the outburst of V1309 Sco was due to the merger of an inspiraling binary system of 1–2 M$_\odot$ (Mason et al. 2010; Tylenda et al. 2011; Pejcha 2014), links could be made between red novae and merger events (Tylenda et al. 2011), including the more massive (3–10 M$_\odot$) proposed mergers V838 Mon (Bond et al. 2003; Sparks et al. 2008) and M31-LRN-2015 (Dong et al. 2015; MacLeod et al. 2017; Blagorodnova et al. 2020). The spectra of these events change dramatically with time, starting with narrow Balmer emission lines on top of a rather featureless blue continuum, and evolving to a cool, dusty, molecular-band-dominated spectrum. Other well-known mergers of even more massive stars include NGC 4490-OT at $\sim$ 30 M$_\odot$ (Smith et al. 2016b; Pastorello et al. 2019), M101-2015OT1 at $\sim$18 M$_\odot$ (Blagorodnova et al. 2017; Goranskij et al. 2016), and SNHunt248 as large as 60 M$_\odot$ (Mauerhan et al. 2018). The light curves of these objects show prominent double or multiple peaks, with more massive progenitors linked with brighter peak magnitudes and a longer duration between peaks (Smith et al. 2016b).

Some intermediate-luminosity transients cannot be strictly classified into one of the three groups discussed above. For instance, UGC 2773-OT exhibited [Ca II] and Ca II emission in its spectra, similar to the SN 2008S-like events, but appears to have had a luminous, blue progenitor and a slow rise to peak luminosity akin to the Great Eruption of η Car (Smith et al. 2010, 2016a; Foley et al. 2011). Moreover, η Car — the quintessential LBV giant eruption — showed prominent

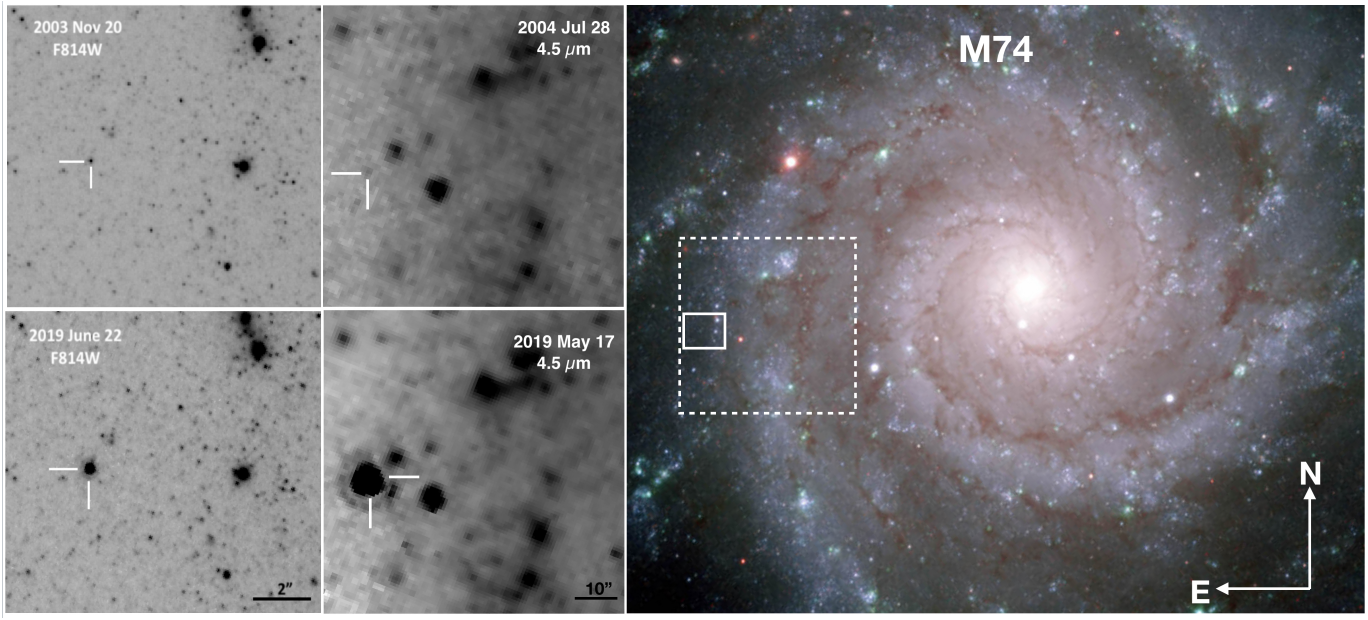

Figure 1. Pre- and post-eruption images of AT 2019krl with *HST* *F*814*W* (two left panels) and *Spitzer*/IRAC 4.5 μm (middle panels). AT 2019krl is indicated by the white tick marks, and the panels have the same orientation with north up, east to the left. The scale of the *HST* (solid rectangle) and *SST* (dashed rectangle) images is shown against the Gemini/GMOS color image on the right.

[Ca II] emission and molecular absorption in light-echo spectra (Prieto et al. 2014; Smith et al. 2018), plus prodigious dust formation and other features that are also attributed to ILRTs. Similarly, the optical spectra of SN 2002bu evolved from the appearance of an LBV to that of a SN 2008S type, and observations over a decade after the outburst are inconclusive about whether the event was terminal (Szczygieł et al. 2012).

Here we present another case of an intermediate-luminosity transient that shows outburst characteristics of belonging to both LBV and SN 2008S-like events. In this case, however, a luminous blue progenitor is clearly detected in pre-eruption data. AT 2019krl (ZTF19abehwhj) was discovered on 2019 July 07 (Ho 2019) by the Zwicky Transient Facility (ZTF; Bellm et al. 2019) in the nearby spiral galaxy M74 (NGC 628). It was later classified as either a Type IIn supernova or an LBV in outburst, based on an optical spectrum taken on 2019 July 8.4 that showed strong, complex Hα emission with a narrow (130 km s^{-1}) and an intermediate (2000 km s^{-1}) width component (Andrews et al. 2019). M74 has been host to the well-studied SNe 2002ap, 2003gd, and 2013ej which have resulted in a rich dataset of archival imaging in the optical and infrared. From ground-based imaging using 20 reference Gaia DR2 (Gaia Collaboration et al. 2018) stars we obtained an absolute position of AT 2019krl of α(J2000) = $01^h36^m49^s.633$, δ(J2000) = $15°46'46''.32$. A subsequent search of the *Spitzer* Heritage Archive found that the object was detected in archival *Spitzer Space Telescope* (*SST*; Werner et al. 2004; Gehrz et al. 2007) images and appeared as a bright source in the last observational epoch on 2019 May 17, approximately two months prior to the optical discovery (Szalai et al. 2019). Adopting a distance modulus to M74 of $\mu = 29.95 \pm 0.03$ (stat.) ± 0.07 (syst.) mag ($d = 9.77 \pm 0.17 \pm 0.32$ Mpc; McQuinn et al. 2017, which is consistent with the distance determined by Kreckel et al. 2017 using the planetary nebula luminosity function), the absolute magnitude of AT 2019krl in the brightest epoch from *Spitzer* was $M_{4.5\,\mu\mathrm{m}} = -18.4$. The combination of bright mid-infrared (MIR) emission, low optical brightness, and narrow Balmer emission suggested that AT 2019krl was likely one of the intermediate-luminosity transients discussed above.

We outline the observations and data reduction in Section 2, and discuss the light curve and spectroscopic evolution of the progenitor and event in Section 3. Section 4 discusses the constraints on the progenitor and explosion from the data, and Section 5 compares these with other intermediate-luminosity transient types. We end with concluding remarks in Section 6.

2. OBSERVATIONS

2.1. *HST Photometry*

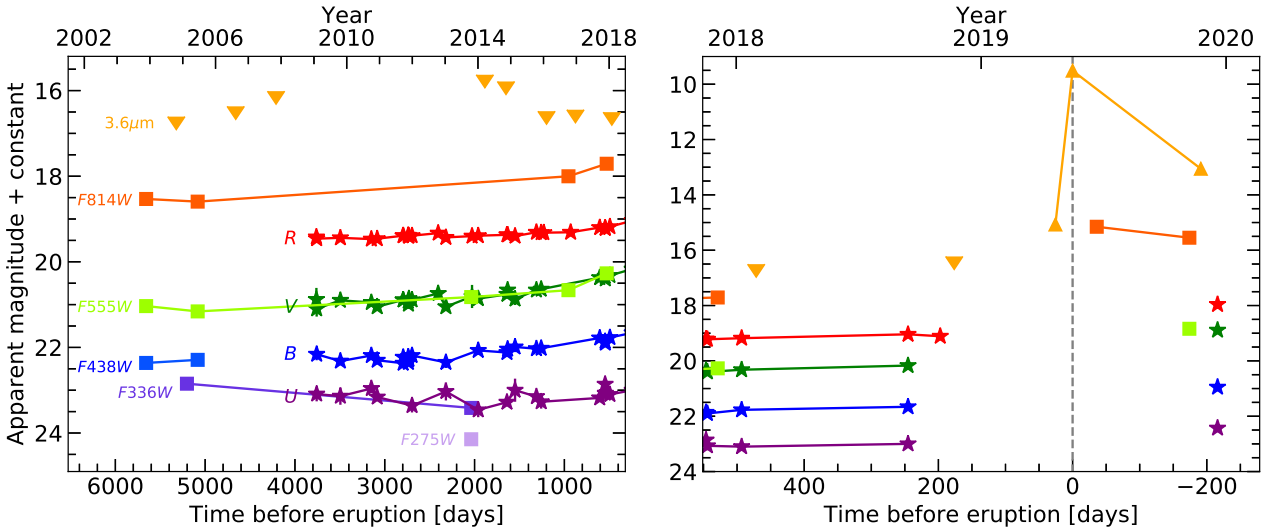

Figure 2. Optical and infrared light curves of AT 2019krl. *UBVR* data are from the LBT and other data are from *HST* and *Spitzer*. The light curves have been shifted by constants for ease of viewing. The left panel shows the light curve of the progenitor, while the right panel focuses on the eruption. The date of our brightest *Spitzer* epoch is indicated by a vertical dashed line, and upper limits from the *Spitzer* measurements, stacked in one-year bins, are indicated by downward pointing triangles. The upper limits are similar in the 3.6 μm and 4.5 μm bands. The data are presented in Tables 1, 2, and 3.

The site of the transient has been imaged many times before with *HST*. In addition, *HST*/ACS *F*814*W* observations of M74 obtained on 2019 June 22 (PI: D. Sand) serendipitously imaged AT 2019krl two weeks before the discovery report was issued (Ho 2019). Using this post-outburst observation, we could easily isolate the progenitor star in pre-outburst archival *HST* images.

Pre-transient ACS/WFC data were obtained from programs GO-9796 (PI: J. Miller; 2003 November 20), GO-10402 (PI: R. Chandar; 2005 June 16), and GO-15645 (PI: D. Sand; 2019 June 22). Several epochs of WFC3/UVIS are available, including from programs GO-13364 (PI: D. Calzetti; 2013 October 17), GO-13773 (PI: R. Chandar; 2014 October 14), GO-14668 (PI: A. Filippenko; 2016 October 04), and GO-15166 (PI: A. Filippenko; 2017 December 04). Additionally, another post-explosion epoch was taken with WFC3/UVIS on 2019 November 07 (GO-15151; PI: S. Van Dyk). One epoch of WFPC2/WF3 data was also obtained from GO-10402 (PI: R. Chandar; 2005 February 16). The data were all obtained from the Mikulski Archive for Space Telescopes (MAST[1]) with standard pipeline calibrations applied. See Table 1. In Figure 1 we show the transient location in a pre-eruption image from 2003, and one post-eruption image from 2019. We analyzed these data with DOLPHOT[2] (Dolphin 2000, 2016), after using AstroDrizzle (Hack et al. 2012) to produce drizzled image mosaics and to flag cosmic-ray hits in the individual frames. We used the recommended parameters for DOLPHOT and adopted values for the parameters `FitSky`=3 and `RAper`=8 for the photometry. We present the *HST* photometry on the Vega scale in Table 1.

[1] https://archive.stsci.edu/
[2] http://americano.dolphinsim.com/dolphot/

2.2. *LBT Photometry*

Observations of M74, including the position of AT 2019krl, were obtained as part of the Large Binocular Telescope (LBT) Search for Failed Supernovae (Kochanek et al. 2008). As part of this survey, *UBVR* images of M74 were obtained between 2008 and 2019 using the Large Binocular Cameras (LBC; Giallongo et al. 2008) on the LBT. The data reduction and image processing are described by Gerke et al. (2015) and Adams et al. (2017). In summary, the best images are combined to make a reference image, and the individual epochs are analyzed using the ISIS image-subtraction package (Alard & Lupton 1998; Alard 2000). The difference imaging provides a light curve of the variable flux that is unaffected by crowding. The mean flux of the source in the reference image is subject to the effects of crowding and is less well-determined.

The data are calibrated using stars in the Sloan Digital Sky Survey (SDSS; Ahn et al. 2012) and transformed to $UBVR_C$ Vega magnitudes using the conversions reported by Jordi et al. (2006). These calibrations are accurate to 0.1 mag or better. The uncertainties in the transient light curve are estimated using the variance of

Table 1. *HST* observations

Date	Filter	Instrument	VegaMAG[a]
2003-11-20	*F435W*	ACS/WFC	24.363±0.012
	F555W	ACS/WFC	24.035±0.016
	F814W	ACS/WFC	23.332±0.015
2005-02-16	*F336W*	WFPC2/WF3	23.848±0.121
2005-06-16	*F435W*	ACS/WFC	24.291±0.042
	F555W	ACS/WFC	24.159±0.045
	F814W	ACS/WFC	23.394±0.026
2013-10-17	*F275W*	WFC3/UVIS	24.646±0.115
	F336W	WFC3/UVIS	24.414±0.094
	F555W	WFC3/UVIS	23.824±0.020
2014-10-14	*F547M*	WFC3/UVIS	23.713±0.044
	F657N	WFC3/UVIS	21.089±0.022
2016-10-04	*F555W*	WFC3/UVIS	23.663±0.021
	F814W	WFC3/UVIS	22.802±0.024
2017-12-04	*F555W*	WFC3/UVIS	23.270±0.018
	F814W	WFC3/UVIS	22.509±0.022
2019-06-22	*F814W*	ACS/WFC	19.953±0.003
2019-11-07	*F555W*	WFC3/UVIS	21.840±0.025
	F814W	WFC3/UVIS	20.349±0.020

[a]DOLPHOT magnitudes obtained from the *HST* data.

light curves extracted from nearby source-free regions, as these empirical uncertainties will include any systematic contributions to the uncertainties beyond simple Poisson errors. The LBT photometry is listed in Table 2.

2.3. *Spitzer Photometry*

There have been many observations of M74 in the 3.6 and 4.5 μm imaging channels ([3.6] and [4.5]) of the Infrared Array Camera (IRAC; Fazio et al. 2004) onboard *Spitzer* since 2004 as part of several observing programs (PID 159, PI: R. Kennicutt; PID 3248, PI: W. P. Meikle; PID 30494, PI: B. Sugerman; PID 40010, PI: M. Meixner), including extensive coverage since 2014 by the SPitzer InfraRed Intensive Transients Survey (SPIRITS; PIDs 10136, 11063, 13053, 14089; PI: M. Kasliwal) through the end of 2019. Pre-discovery photometry was presented by Szalai et al. (2019) up until the infrared (IR) peak of the transient on 2019 May 17, including the upper limits of the nondetections at 5.8 μm and 8.0 μm of 5 μJy and 15 μJy, respectively.

As part of SPIRITS, the post-basic calibrated data (PBCD) level images were downloaded from the *Spitzer* Heritage Archive[3] and *Spitzer* Early Release Data Service[4] and processed through an automated image-subtraction pipeline (for details, see Kasliwal et al. 2017). For reference images, we used the images taken on 2004 July 28 for the *Spitzer* Infrared Nearby Galaxies Survey (SINGS; Kennicutt et al. 2003). We performed aperture photometry on the difference images using a 4 mosaicked-pixel (2.″4) aperture and background annulus from 4–12 pixels (2.″4–7.″2). The extracted flux is multiplied by the aperture corrections of 1.215 for [3.6] and 1.233 for [4.5] as described in the IRAC Instrument Handbook[5]. To estimate the photometric uncertainties, we performed photometry with the same parameters as above in a grid of apertures spanning a 32″ box with 8″ spacing centered at the location of each candidate, excluding the central aperture. We adopt a robust estimate of the root-mean-square (rms) uncertainty in the distribution of flux measurements for the aperture grid ($0.5 \times [85^{\rm th} - 16^{\rm th}$ percentile]) as representative of the 1σ uncertainties in our photometry.

In the 2004 reference images used for subtraction, a possible quiescent counterpart is visible at both [3.6] and [4.5]. Our aperture photometry gives low-significance measurements of $F_{\nu,[3.6]} = 4.6 \pm 4.5$ and $F_{\nu,[4.5]} = 7.1 \pm 3.6\,\mu$Jy, consistent with 2005 January 15 measurements by Szalai et al. (2019). Given the limited spatial resolution of *Spitzer*/IRAC and the complicated background emission, it is not possible to rule out that the emission at the site is due to confusion with nearby, unrelated sources. Thus, we infer 3σ limits on the IR flux of the precursor in 2004 of $F_{\nu,[3.6]} < 14$ and $F_{\nu,[4.5]} < 11\,\mu$Jy. We adopt our difference imaging measurements throughout the rest of this work with the caveat that they may underestimate the true source flux. We convert our flux measurements to Vega-system magnitudes using the zero-magnitude fluxes presented for each IRAC channel in the IRAC Instrument Handbook and list our photometry in Table 3.

2.4. *Spectroscopy*

Multiple long-slit optical spectra were taken of AT 2019krl with various telescopes/instruments between July and November 2019. These include one epoch with Binospec (Fabricant et al. 2019) on the 6.5 m MMT telescope, one epoch with the Kast double spectrograph (Miller & Stone 1993) mounted on the Shane 3 m telescope at Lick observatory, one epoch with the Goodman spectrograph (Clemens et al. 2004)

[3] https://sha.ipac.caltech.edu/applications/Spitzer/SHA/

[4] http://ssc.spitzer.caltech.edu/warmmission/sus/mlist/archive/2015/msg007.txt

[5] http://irsa.ipac.caltech.edu/data/SPITZER/docs/irac/iracinstrumenthandbook/

Table 2. AT 2019krl LBT photometry[a]

MJD	U	B	V	R
	mag	mag	mag	mag
54859	–	–	23.58 ± 0.27	22.42 ± 0.06
54862	23.59 ± 0.17	24.16 ± 0.14	23.80 ± 0.18	22.46 ± 0.01
55126	23.64 ± 0.20	24.32 ± 0.06	23.60 ± 0.07	22.44 ± 0.01
55471	23.46 ± 0.08	24.19 ± 0.04	23.65 ± 0.05	22.47 ± 0.01
55536	23.66 ± 0.05	24.30 ± 0.04	23.75 ± 0.04	22.46 ± 0.01
55825	–	24.37 ± 0.12	23.59 ± 0.06	22.39 ± 0.02
55826	–	24.23 ± 0.04	23.59 ± 0.03	22.39 ± 0.02
55882	–	24.22 ± 0.07	23.62 ± 0.06	22.38 ± 0.02
55884	–	24.35 ± 0.08	23.69 ± 0.11	22.40 ± 0.01
55889	–	24.28 ± 0.07	23.56 ± 0.05	22.40 ± 0.02
55924	23.86 ± 0.16	24.19 ± 0.06	23.59 ± 0.03	22.39 ±0.01
56215	–	–	23.44 ± 0.13	22.33 ± 0.07
56301	23.53 ± 0.21	24.35 ± 0.13	23.75 ± 0.07	22.43 ± 0.02
56592	–	–	23.51 ± 0.27	22.40 ± 0.03
56661	23.96 ± 0.17	24.07 ± 0.04	23.56 ± 0.05	22.39 ± 0.01
56981	23.78 ± 0.09	24.12 ± 0.03	23.46± 0.03	22.37 ± 0.01
56988	–	24.04 ± 0.08	23.36 ± 0.07	22.37 ± 0.01
57071	23.50 ± 0.27	23.99 ± 0.12	23.57 ± 0.14	22.40 ± 0.03
57309	23.65 ± 0.07	24.03 ± 0.06	23.36 ± 0.03	22.31 ± 0.01
57362	23.77 ± 0.16	24.02 ± 0.07	23.34 ± 0.06	22.32 ± 0.02
57391	–	–	–	22.32 ± 0.03
57690	–	–	–	22.31 ± 0.02
58014	23.68 ± 0.05	23.78 ± 0.04	23.07 ± 0.03	22.20 ± 0.01
58074	23.36 ± 0.12	23.86 ± 0.04	23.04 ± 0.02	22.21 ± 0.01
58076	23.57 ± 0.16	23.90 ± 0.05	23.10 ± 0.08	22.22 ± 0.02
58127	23.60 ± 0.11	23.77 ± 0.04	23.02 ± 0.03	22.18 ± 0.01
58375	23.50 ± 0.06	23.66 ± 0.02	22.87 ± 0.03	22.04 ± 0.01
58423	–	–	–	22.11 ± 0.03
58837	22.93 ± 0.10	22.95 ± 0.02	21.59 ± 0.01	20.96 ± 0.01

[a] Magnitudes are in the Vega system.

on the 4.1 m SOAR telescope, one epoch taken with the DEep Imaging Multi-Object Spectrograph (Faber et al. 2003, DEIMOS) on the 10 m Keck-II telescope at Maunakea, and a final epoch with the Multi-Object Double Spectrographs (Pogge et al. 2010, MODS) on the twin 8.4 m LBT at Mount Graham International Observatory. These spectra were reduced using standard techniques, including bias subtraction, flat fielding, cosmic ray rejection, local sky subtraction, and extraction of one-dimensional spectra. The MMT data were reduced using the Binospec pipeline (Kansky et al. 2019). Most observations had the slit aligned along the parallactic angle to minimize differential light losses (Filippenko 1982). Flux calibration was done with standard-star observations taken on the same night at similar airmass.

A pre-outburst spectrum is serendipitously available from observations using the Very Large Telescope/Multi Unit Spectroscopic Explorer (VLT/MUSE) spectrograph (Bacon et al. 2010) as part of the PHANGS[6]-MUSE survey (E. Emsellem et al., in prep.). This optical integral field unit provides a $1'\times\ 1'$ field of view with $0''.2$ pixels and a typical spectral resolution of $\sim$2.5 Å over the nominal wavelength range, covering 4800–9300 Å. Observations of M74 (Kreckel et al. 2018, 2019) were taken on 2018 November 13 and targeted the source position in three rotations, alternating with two sky pointings, for a total on-source integration time of 50 min. Data reduction is carried out using a pipeline

[6] Physics at High Angular resolution in Nearby GalaxieS; http://www.phangs.org

Table 3. AT 2019krl *Spitzer* Photometry

MJD	[3.6] Diff. Flux (μJy)	Error (μJy)	[4.5] Diff. Flux (μJy)	Error (μJy)	[3.6] (mag)	Error (mag)	[4.5] (mag)	Error (mag)
53211.82	1.2	1.9	1.1	0.9	> 19.3	···	> 19.4	···
53385.98	−1.3	1.8	−2.8	2.1	> 19.3	···	> 18.5	···
53960.85	0.7	1.7	−0.4	1.1	> 19.4	···	> 19.1	···
54328.12	0.1	3.2	−4.5	2.8	> 18.6	···	> 18.2	···
54491.19	−2.5	3.1	−3.8	2.5	> 18.7	···	> 18.3	···
56734.98	0.6	3.2	−1.3	12.6	> 18.6	···	> 16.7	···
56936.57	···	···	3.4	1.5	···	···	> 18.8	···
56970.14	−0.4	2.8	0.0	1.3	> 18.8	···	> 19.0	···
57312.98	−1.1	2.8	···	···	> 18.8	···	···	···
57320.53	···	···	1.0	1.8	···	···	> 18.6	···
57334.24	0.9	3.3	0.0	1.7	> 18.6	···	> 18.7	···
57474.90	1.3	2.1	···	···	> 19.1	···	···	···
57482.44	4.7	21.8	2.1	2.9	> 16.6	···	> 18.2	···
57503.57	0.7	4.3	−1.7	17.1	> 18.3	···	> 16.3	···
57680.70	4.2	2.4	3.6	2.8	> 19.0	···	> 18.2	···
57695.05	−0.3	2.3	−0.3	1.7	> 19.0	···	> 18.7	···
57855.38	1.3	3.3	···	···	> 18.6	···	···	···
58054.61	2.9	1.7	2.5	0.9	> 19.4	···	> 19.3	···
58242.87	5.8	3.2	10.4	20.0	> 18.7	···	> 16.2	···
58427.87	2.8	2.1	8.2	1.2	> 19.1	···	18.35	0.16
58459.75	4.9	4.0	10.5	2.7	> 18.4	···	18.08	0.28
58594.60	16.6	1.8	29.8	2.1	18.07	0.12	16.95	0.08
58620.24	2779.3	15.1	4121.7	25.4	12.51	0.01	11.60	0.01
58811.34	106.1	3.1	216.4	1.3	16.06	0.03	14.80	0.01

wrapping around the MUSE data reduction pipeline (Weilbacher et al. 2020) and developed by the PHANGS team.[7] A log of the spectroscopic observations is given in Table 4.

3. ANALYSIS

3.1. *Metallicity*

Using the adopted distance of 9.77 Mpc (McQuinn et al. 2017), AT 2019krl is located roughly 5.4 kpc from the center of M74. Assuming the oxygen abundance gradient in M74 is 12 + log[O/H]= (8.834±0.069)+(−0.044±0.011)×R(dex kpc^{-1}) (Berg et al. 2015) we derive 12 + log[O/H] = 8.59 ± 0.1, a value consistent with the solar oxygen abundance of 8.69 ± 0.05 (Asplund et al. 2009). Therefore, we assume the metallicity at the location of AT 2019krl is approximately solar.

3.2. *Extinction*

The equivalent width (EW) of the Na I D $\lambda\lambda$5889, 5896 absorption feature is often used following the prescription of Poznanski et al. (2012) to estimate the extinction of an extragalactic transient, although Phillips et al. (2013) have cautioned against using this relation to obtain extinction estimates. Unfortunately, the Na I D lines in AT 2019krl are seen only in emission (Figure 3), likely from a contribution from the surrounding circumstellar medium (CSM). For core-collapse SNe the observed color, for example, can be used to estimate the extinction, since the intrinsic colors of such SNe are relatively well defined (e.g., Drout et al. 2011; Stritzinger et al. 2018, although see de Jaeger et al. 2018). Since outbursts such as AT 2019krl are not well understood, this is also not a viable option.

However, we can instead attempt to constrain the reddening $E(B-V)$ of AT 2019krl from the nearby stellar population. Using a technique similar to that outlined by Kreckel et al. (2013), we use penalized pixel-fitting (Cappellari & Emsellem 2004; Cappellari 2017) to determine the linear combination of Bruzual & Charlot (2003) simple stellar population templates that best fits an integrated 100 pc wide annular integrated spectrum. This fit requires a third order multiplicative polynomial, which

[7] https://github.com/emsellem/pymusepipe

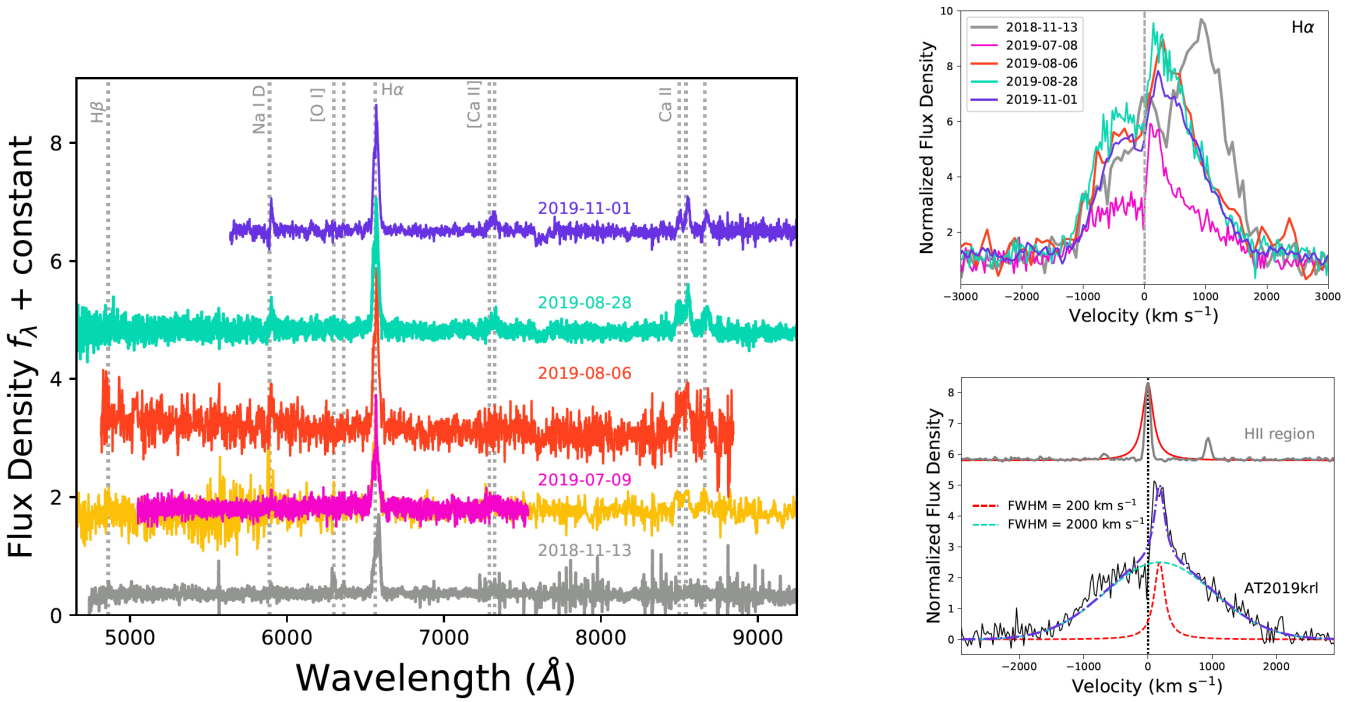

Figure 3. Left: Spectroscopic evolution of the progenitor (gray) and eruption of AT 2019krl. A list of the spectroscopic observations is presented in Table 4. The spectra have not been corrected for extinction, and prominent emission lines are marked with gray dotted lines. Right top: The evolution of the Hα emission line. The epochs have been normalized to the continuum and scaled to match the blue-side peak. The excess in the 2018 pre-eruption spectrum emission (gray) at $\sim$1000 km s^{-1} is [N II] λ6584. Right bottom: Plot of the Hα and H II emission lines from MMT/Binospec. The H II region lines are fully resolved and the peak of Hα is redshifted from zero velocity. The Hα component can be fit by a narrow Lorentzian and wide Gaussian.

agrees well in shape with a Calzetti et al. (2000) attenuation law. From this comparison we obtain a value of $E(B-V)_{\rm total} = 0.12$ mag, after including the Milky Way line-of-sight reddening toward M74 of $E(B-V)_{\rm MW} = 0.062$ mag (Schlafly & Finkbeiner 2011). This is only a lower limit, as circumstellar extinction around the transient may be much higher, but likely provides us with a reasonable estimate of total foreground extinction which we will use throughout the rest of the paper.

3.3. *Light curve and color evolution*

The optical light curves, shifted for ease of viewing, are shown in Figure 2, with the photometry listed in Tables 1, 2, and 3. The absolute magnitudes of the progenitor at the first epoch in 2003 are roughly $M_{F435W} = -6.0$ mag, $M_{F555W} = -6.3$ mag, and $M_{F814W} = -6.8$ mag corrected for $E(B-V)_{\rm total} = 0.12$ mag. In 2013 the progenitor is somewhat brighter with $M_{F275W} = -5.9$ mag, $M_{F336W} = -6.1$ mag, and $M_{F555W} = -6.5$ mag. From our *HST* photometry taken in 2017, we see that $M_{F555W} = -7.0$ mag, or almost a magnitude brighter than in 2003, and that between 2017 September and 2018 September it brightens by another 0.1–0.2 mag. The LBT data, which begin in 2009, show a fairly flat evolution up until late 2017, eliminating any other major eruptions in the decade previous.

The 3.6 μm magnitudes are also shown in Figure 2. Only upper limits are obtained for the majority of the early evolution, but similar to the optical data, the 3.6 μm and 4.5 μm data do not seem to indicate any major outbursts between 2004 and 2018. There is a noticeable increase from 2018 December to 2019 April as the 4.5 μm luminosity increases from -11.9 to -13.0 mag. Finally, on 2019 May 17 we obtain our highest luminosities of $M_{3.6\,\mu{\rm m}} = -17.5$ mag, and $M_{4.5\,\mu{\rm m}} = -18.4$ mag. From these *Spitzer* data, we can constrain the peak of the outburst to be between 2019 April 21 and May 17. The peak was not observed in the optical data owing to Sun constraints.

We only obtained a handful of observations after discovery. The photometry from the ACS/$F814W$ image taken on 2019 June 22 reveals a luminosity of $M_{F814W} = -10.2$ mag, which then falls to -9.9 mag by 2019 November 07. Similarly, $M_{3.6\,\mu{\rm m}}$ and $M_{4.5\,\mu{\rm m}}$ have dropped to -13.9 and -15.2 mag, respectively, by

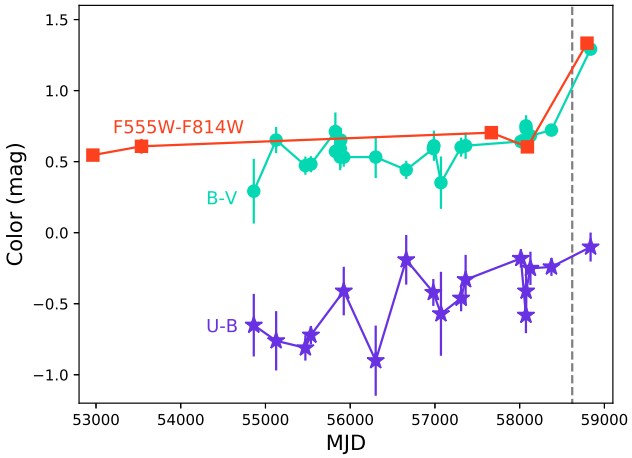

Figure 4. Color evolution of the progenitor and outburst of AT 2019krl. As in other figures the date of our brightest *Spitzer* epoch is indicated by a vertical dashed line and all data have been corrected for $E(B-V) = 0.12$ mag.

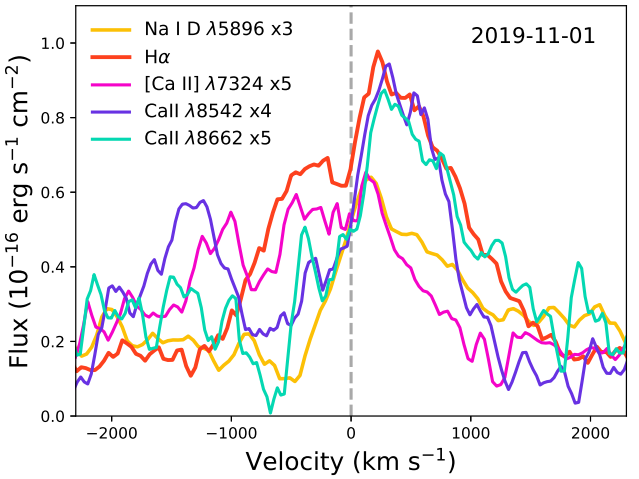

Figure 5. Velocities of prominent emission lines in the 2019 November LBT spectrum. The lines have been multiplied by a constant indicated in the legend.

2019 November, corresponding to a decrease of roughly 0.02 mag day^{-1}.

As shown in Figure 4, the source steadily becomes redder, with a larger change in the color of the bluer bands. The $U-B$ color evolves from roughly -0.6 to -0.1 mag, the $B-V$ from 0.4 to 0.8 mag, and the *HST* $V-I$ color remains fairly flat at ~ 0.7 mag. After the eruption the *HST* $V-I$ and $B-V$ colors both jump to roughly 1.4 mag, while $U-B$ gets redder by only 0.1 mag. This indicates that the post-eruption object was much redder than the pre-eruption progenitor. We will discuss how the light curve and color evolution can be used to infer progenitor and explosion properties in Section 4 below.

3.4. *Spectroscopic Evolution*

The spectroscopic evolution of AT 2019krl, including a progenitor spectrum from ~ 6 months prior to eruption, are shown in Figure 3 and listed in Table 4. To confirm the rest velocities of the components which appear redshifted with respect to the zero velocity of the galaxy, we have also plotted the profile of a nearby H II region along with the narrow Lorentzian function used to fit the Hα line of the transient, as we discuss below. This exercise shows that not only is the Hα of the H II region centered at zero velocity and there is indeed a true velocity offset, but that we are also fully resolving the narrow component in the Hα profile of AT 2019krl, and that it is broader than the H II region lines.

All spectra exhibit prominent Hα emission, but are otherwise almost featureless. As the upper-right plot in Figure 3 shows, the Hα emission line in all epochs appears to be multipeaked, with an absorption feature near 0 km s^{-1}. Our earliest spectrum on 2019 July 08 from the MMT is shown in the lower right of Figure 3, and can be reproduced by a combination of a broad Gaussian with a full-width a half-maximum intensity (FWHM) = 2000 km s^{-1} and a narrow Lorentzian with a FWHM = 200 km s^{-1}, both centered at 180 km s^{-1}, although there is still a slight excess relative to the blue fit on the blue wing. The strong Ca II NIR triplet, which is not present in the progenitor, as well as Na I D $\lambda\lambda$5890, 5896 and very weak [Ca II] are all seen in emission in the post-eruption spectra.

A comparison of the prominent emission lines from our last epoch on 2019 November 01 is shown in Figure 5, where some lines have been scaled for ease of viewing. Both Hα and the weak [Ca II] λ7324 line appear to have an excess of emission on the blue side which is not seen in the Ca II NIR triplet, likely due to a blueshifted absorption line. On the other hand, while the red side of Ca II NIR and Hα are qualitatively similar, neither [Ca II] λ7324 nor the Na I D λ5896 lines show an excess on the red side. The noticeable absorption in the λ8662 line, and to a lesser extent the λ8542 line, at -650 km s^{-1}, which is offset by $\sim$ 800–900 km s^{-1} from the peak of the line, may indicate multiple locations for the various line emissions. This could be explained with an eruption in a dense, equatorial CSM, where the ejecta could expand much faster at the poles, yet slower in the plane of the disk where the [Ca II] emission would arise. A similar trend of faster Hα and Ca II and slower [Ca II] was seen in the post-eruption spectra of UGC 2773-OT which may also have a bipolar nebula (Smith et al. 2016a).

Table 4. Optical Spectroscopy of AT 2019krl

Date	MJD	Telescope +Instrument	R $\lambda/\Delta\lambda$	Exp. (s)
2018-11-13	58435.41	VLT+MUSE	2600	3000
2019-07-08	58672.46	MMT+Binospec	3100	1800
2019-07-09	58673.95	Lick Shane+Kast	770	3600
2019-08-06	58701.35	SOAR+Goodman	1100	1800
2019-08-28	58723.56	Keck+DEIMOS	1875	1200
2019-11-01	58788.19	LBT+MODS	2000	900

4. RESULTS

4.1. *Constraints on the progenitor*

The *HST* and LBT data, along with the MUSE spectrum of the progenitor of AT 2019krl, allow us to thoroughly investigate the properties of the star that gave rise to this transient. Without a reliable value for the local extinction, our conservative choice of $E(B-V) = 0.12$ mag will only provide lower limits to the mass and temperature of the progenitor, but will allow us to rule out certain classes of stars.

In Figure 6 we show the optical spectral energy distributions (SEDs) of the progenitor from photometry in 2005 (*HST* only), 2013 (*HST* and LBT), and 2017 (*HST* and LBT). These epochs were chosen owing to the availability of the ultraviolet (UV) and U-band data, which provide the tightest constraints on the masses and temperatures of massive stars. We have attempted to fit the data with ATLAS synthetic spectra of stars of solar metallicity and $\log(g) = 2.0$ (Castelli & Kurucz 2003). From all three epochs we can immediately rule out a cool progenitor, such as a red supergiant (RSG) or an AGB star, as even the minimum fit temperature of 6500 K is too high for those types of stars. The FWHM of 200 km s^{-1} of the narrow Hα component discussed above, which traces the outflow wind velocity of the star, is also faster than typical RSG winds that have average wind velocities of 10–20 km s^{-1} (Mauron & Josselin 2011; Goldman et al. 2017; Beasor & Davies 2018). Moreover, RSGs and AGB stars do not exhibit strong Hα emission.

The 2005 epoch can be best fit by a 11000 K star with $\log(L/L_\odot) = 4.4$, although there is excess emission in the $F814W$ band that cannot be fit with just a single stellar model. In the subsequent two epochs the progenitor appears to cool and become more luminous with time, dropping to $T_{\rm eff} = 6500$ K with a higher luminosity of $\log(L/L_\odot) = 4.6$ by 2017. This is, of course, a lower limit, since any additional extinction (host or circumstellar) would raise both the temperature and luminosity. For instance, acceptable fits could be made to the 2005 data with a 17,000 K model and $E(B-V) = 0.6$ mag. Note that we have not attempted to fit the R-band data in 2013 and 2017, as this filter contains the bright Hα emission seen in the progenitor spectrum.

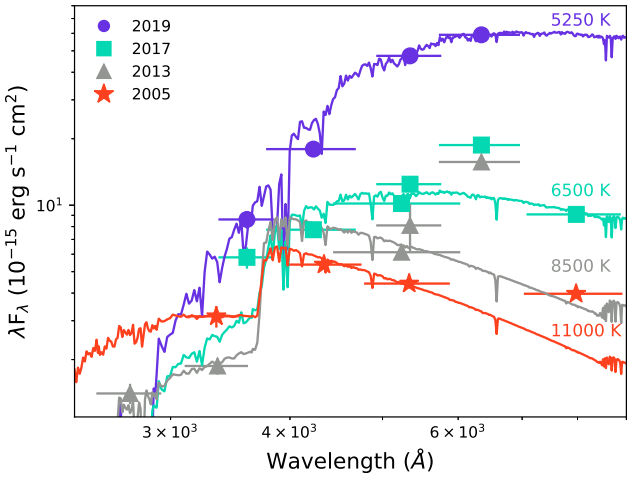

Figure 6. Evolution of the SED of AT 2019krl from *HST* (filled symbols) and LBT (open symbols) observations. The data have only been corrected for $E(B-V) = 0.12$ mag. For comparison ATLAS synthetic spectra of stars with solar metallicity and $\log(g) = 2.0$ are shown.

For comparison, yellow supergiants (YSGs) have $7500\,{\rm K} \gtrsim T_{\rm eff} \gtrsim 4800\,{\rm K}$ and $\log(L/L_\odot) > 4.36$, with LBVs and blue supergiants (BSGs) exhibiting significantly warmer temperatures. LBVs in their cool outburst states typically have temperatures around 6000–10,000 K. The SED fits therefore indicate that the progenitor star was either a rather hot YSG, a quite cool BSG, or an LBV-like star in a cool phase. The $F555W - F814W$ color evolution (shown in Figure 4) is too blue for an RSG, and is more consistent with a BSG or YSG.

In Figure 7 we compare the 2005 and 2013 *HST* data to the MESA Isochrones & Stellar Tracks (Choi et al. 2016; Dotter 2016, MIST[8]) to help constrain the progenitor masses. For each epoch we have determined the best-fit mass for three possible extinction values, with the lowest value of $A_V = 0.4$ mag corresponding to that used throughout this paper. The colors indicate the main sequence (MS, red), supergiant branch (SGB, teal), and helium core burning (HeCB, yellow) phases, and the solid, dotted, and dashed lines show the various mass tracks. In both 2005 and 2013 we find a lower limit to the progenitor mass of 13.5 $M_\odot$; however, the data with the largest amount of extinction applied yield

[8] http://waps.cfa.harvard.edu/MIST/

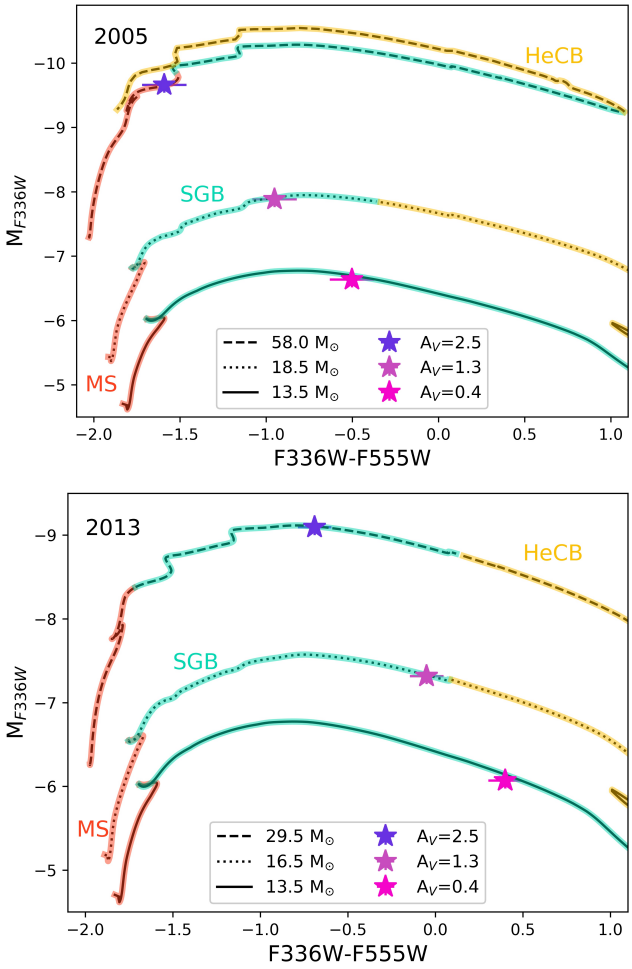

Figure 7. Color-magnitude diagram of the progenitor of AT 2019krl (stars) in 2005 (top) and 2013 (bottom) with varying degrees of extinction applied. The main sequence (MS, red), supergiant branch (SGB, teal), and helium core burning (HeCB, yellow) are highlighted. The best-fit masses corresponding to each extinction value are shown as a solid, dotted, and dashed line, respectively. At no time was the SED as red as an AGB star or RSG.

a progenitor mass of 58 $M_\odot$ in 2005 and only 29.5 $M_\odot$ in 2013.

To illustrate how the progenitor mass estimate changes depending on the epoch, we show the evolution of the source in M_{F555W} and $F555W - F814W$ in Figure 8. Similar to the SED fits, there is a trend to redder colors with time. This translates to shifts in progenitor mass estimates from around 13 $M_\odot$ to 15 $M_\odot$, but also a shift in the inferred evolutionary stage from SGB to HeCB. This, of course, is not real evolution, as the change to helium core burning takes significantly more time than a mere 15 yr. Instead, it illustrates how changes in the stellar structure due to instability before an eruption can mimic observed evolutionary changes; values for the inferred mass or luminosity from any single epoch of such a transient should therefore be regarded with caution.

Finally, the progenitor spectrum provides valuable clues about the physical state of the star prior to eruption. The spectrum is dominated by broad Hα with wings extending to roughly $\pm$ 2000 km s^{-1}. Strong [N II] λ 6584 emission is present as well, centered at 960 km s^{-1}. Unlike the narrow emission lines of nearby H II regions that have FWHM at the resolution limit of the spectrum of $\sim$ 115 km s^{-1}, the [N II] λ5755, λ6584 and [O I] $\lambda\lambda$6300, 6363 lines have FWHM = 900 km s^{-1}. This points to emission of N-rich CSM, which is only produced around massive stars; for instance, the outer ejecta of η Car show strong [N II] emission (Smith & Morse 2004).

While the colors of the progenitor are consistent with a BSG, YSG, or cool LBV, line widths of 2000 km s^{-1} are not seen in those stars even if Hα is present. LBVs occasionally can show strong Hα emission with high velocities, for instance the 2009 September outburst of SN 2009ip (Smith et al. 2010). However, in the case of SN 2009ip, the line core was only 550 km s^{-1}, with broad wings extending out to 2000 km s^{-1}, while in the case of AT 2019krl the bulk of the emission extends well beyond 1000 km s^{-1}, with wings extending to 2000 km s^{-1}. This suggests the outflow velocities in the progenitor of AT 2019krl are even higher than typical observed LBV outbursts. A similar Hα profile shape, though once again not with such high velocities, was seen in the massive, overcontact binary system RY Scuti, which has a toroidal CSM with a density enhancement on the far side of the system due to mass transfer from a binary companion (Smith et al. 2002). A similar mechanism may be at play in AT 2019krl.

Another class of stars that could possibly show this level of Hα flux are sgB[e] stars, which are easily confused with LBVs in quiescence, since they can appear spectroscopically similar, and have similar temperatures and luminosities. The sgB[e] stars generally show [O I] emission (Aret et al. 2016) which is not seen in the post-eruption spectra of AT 2019krl. It does seem to be present in the pre-eruption spectrum, although this could be a contribution from the surrounding H II region.

4.2. *Post-eruption analysis*

The light-curve peak was unfortunately missed in the optical. However, we can use the change in magnitude in the *Spitzer* MIR fluxes to estimate an approximate peak magnitude in the optical light curve bands. The 4.5 μm

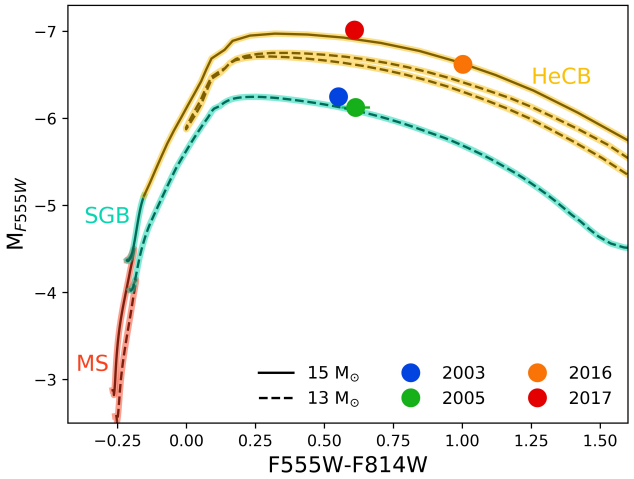

Figure 8. Same as Figure 7 but illustrating the evolution of the progenitor of AT 2019krl within the $F555W - F814W$ color-magnitude diagram with time, corrected for $E(B-V)$=0.12 mag.

data increased by 6.75 mag between 2018 November and the peak in 2019 May. If we assume a similar change in the R-band luminosity from 2018 November, then the peak would be $M_R = -14.6$ mag. If we assume that the color difference between R and other bands remains the same at peak outburst as in late 2017, we can estimate the maximum absolute brightness of $M_{F814W} = -14.3$ mag, $M_V = -13.8$ mag, and $M_{F555W} = -13.5$ mag on 2019 May 17. This is well within the distribution of peak visual-wavelength absolute magnitudes for other SN impostors and/or LBV eruptions (Smith et al. 2011).

Comparison of the Hα evolution (Figure 3) also shows very little change in the Hα line profile from our first spectrum, $\sim$ 60 days after eruption, to the last epoch on $\sim$ 180 days. Additionally, the presence of weak [Ca II] yet relatively strong Ca II emission may provide some insight into the circumstellar environment of AT 2019krl. In SN 2008S (Prieto et al. 2008; Smith et al. 2009) and UGC 2773-OT (Smith et al. 2010) these emission lines were linked to vaporizing dust in the CSM during the outburst. The same may have occurred in AT 2019krl.

5. DISCUSSION

Even though the optical peak of the outburst was missed because AT 2019krl was behind the Sun, the extensive data on the pre-eruption star provides new and important clues into the progenitor and its relationship to the class of SN 2008S-like transients. The observational properties of SN 2008S-like outbursts overlap significantly with other transients, whereas the progenitors remain uncertain and might potentially arise from a variety of dusty objects. Below we discuss how AT 2019krl is like and unlike various transient event classes.

5.1. *Comparison to LBV eruptions*

While LBVs experience low-amplitude, irregular, S-Doradus variations, where the peak of the luminosity is thought to shift from the UV to the optical and the star brightens $\sim$ 1–2 mag, they can also go through a rare form of eruptive mass loss referred to as giant eruptions. Many of the so-called "SN imposters" are generally thought to be nonterminal eruptions of LBVs, similar to the historical eruption of P Cygni or the Great Eruption of η Car (Van Dyk et al. 2000; Smith et al. 2011). During these eruptions the luminosity of the star increases while the temperature drops. The eruptive phase of an LBV can last for years, as in the cases of η Car (Smith & Frew 2011) and UGC 2773-OT (Smith et al. 2016a). Additionally, quiescent or eruptive LBV winds can lie in the 100–600 km s^{-1} range, similar to the resolved narrow Hα component seen in AT 2019krl. The overall appearance of the spectrum in AT 2019krl and SN 2008S-like events — including the [Ca II] and Ca II lines, along with the comparable Hα profiles and line strengths, the inferred temperature, the dusty CSM, and the IR excess — are all consistent with known LBVs.

In Figure 9 we show the B-band light curve of SN 1954J (Tammann & Sandage 1968), thought to be the eruption of a luminous ($M_V \approx -8.0$ mag) and massive (> 25 M$_\odot$) LBV (Van Dyk et al. 2005). The light curves appear similar, except for the small amplitude variability seen in SN 1954J, which is on a fast enough timescale to have been missed by the cadence of the progenitor data for AT 2019krl. Although the masses and luminosities estimated above for AT 2019krl, using the modest extinction of $A_V = 0.4$ mag, are significantly lower than those traditionally associated with LBVs (Smith et al. 2004), only an additional 1–1.5 mag of extinction could easily push AT 2019krl's progenitor to higher masses, as shown in Figure 7. Moreover, recent studies with revised distances have shown that Milky Way LBVs extend to lower initial masses and luminosities than previously thought (Smith et al. 2019).

5.2. *Comparison to SN 2008S type events*

The other class of transients with progenitors that are very bright in the IR are the SN 2008S-like events. Well-studied members of this class include the namesake SN 2008S (Prieto et al. 2008; Botticella et al. 2009; Smith et al. 2009), NGC 300 OT2008-1 (Berger et al. 2009; Bond et al. 2009; Humphreys et al. 2011; Thompson et al. 2009; Kochanek et al. 2012), SN 2002bu (Smith et al. 2011; Szczygieł et al. 2012), PTF10fqs (Kasli-

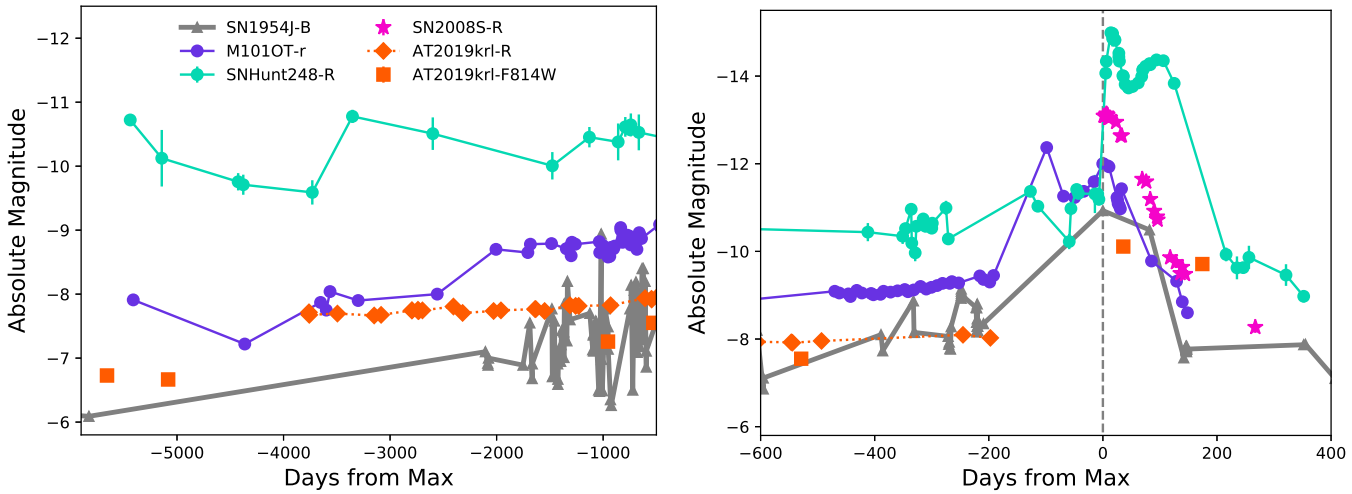

Figure 9. Comparison of the R and $F814W$ light curves of AT 2019krl to other transients. The left panel shows the historical light curves of the progenitors, while the right panel focuses on the eruption. All data have been corrected for their respective $E(B-V)_{\rm MW}$. Data are from Blagorodnova et al. (2017, M101 OT2015-1), Kankare et al. (2015, SNhunt248), Tammann & Sandage (1968, SN1954J), and Botticella et al. (2009, SN 2008S).

wal et al. 2011), AT2017be (Cai et al. 2018), and M51 OT2019-1 (Jencson et al. 2019; Williams et al. 2020).

The SN 2008S-type transients show strong Balmer, Ca II NIR triplet, and [Ca II] emission in their spectra, with outflow velocities on the order of 500–1000 km s^{-1}, similar to many LBV eruptions. In Figure 10 we show the Hα emission at $\sim$70 days post-peak for a sample of SN 2008S-like events. All exhibit fairly smooth Lorentzian profiles with wings extending to $\sim$1000 km s^{-1}; however, for AT 2019krl the emission line is broader and multipeaked. While AT 2019krl shows strong Hα and Ca II NIR, the [Ca II] emission is quite weak. As mentioned above, there may be some connection between [Ca II] and the presence of dust (Prieto et al. 2008; Smith et al. 2009). In particular, dust grains that formed around the progenitor may have evaporated during the sudden luminosity increase of the eruption; see Kochanek (2011) for a full review. This makes sense, as this class of transients has been associated with highly dust-obscured progenitors that only appear in the MIR (Prieto et al. 2008; Thompson et al. 2009). Of course, if the dusty CSM has a nonspherical geometry, then the amount of dust obscuration for the progenitor may vary widely depending on viewing angle (Smith et al. 2009, 2011). An asymmetric CSM around NGC 300-OT was proposed based on optical spectropolarimetry (Patat et al. 2010) and NIR spectroscopy (Ohsawa et al. 2010). If the same is true for AT 2019krl, and the dust is confined to a torus around the progenitor star which we happen to view pole-on, it could appear bright in both the optical and IR. This then begs the question of whether there are two (or more) separate progenitor channels that produce very similar SN 2008S-like transient characteristics, or if instead there is a strong dependency on latitudinal distribution of the scattering dust and the viewing angle. Two different viewing angles through very different columns in the same asymmetric CSM could yield distinct observational classes, leading to the incorrect conjecture that there are two different physical classes of transients if spherical symmetry is assumed. Active galactic nuclei provide a salient example.

In Figure 11 we compare the optical and MIR SEDs for the progenitor of AT 2019krl to the progenitor of SN 20008S and NGC 300-OT. The detection of the optical component only yielded upper limits for SN 2008S and NGC 300-OT, while in every epoch of the AT 2019krl progenitor, we have significant detections. The much closer NGC 300-OT had clear progenitor detections in all of the IRAC bands, while SN 2008S and AT 2019krl had only an upper limit estimated from the 3.6 μm images. The 2018 *Spitzer* data for AT 2019krl are from the post-cryogenic mission only, so there is no way to determine the brightness in the 5.8 μm and 8.0 μm bands, but we have attempted to fit an MIR component with a blackbody temperature of 400 K, between the two temperature values of SN 2008S (Prieto et al. 2008; Thompson et al. 2009, 440K) and NGC 300-OT (Berger et al. 2009, 338K). As we mention above, upper limits were measured for 5.8 μm and 8.0 μm during the cryogenic mission, but the increase in the MIR luminosity of AT 2019krl by 2018 suggests that it would have been detected in these longer wavelength bands.

NGC 300-OT was also detected in the 24 μm MIPS band, while only an upper limit could be derived

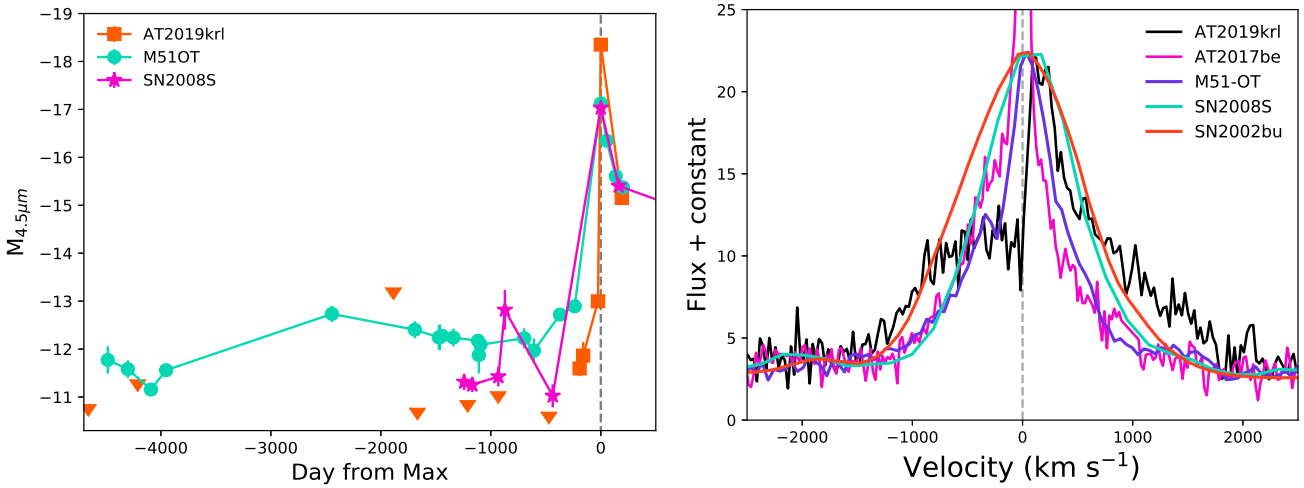

Figure 10. Left: *Spitzer* 4.5 μm light curves of the progenitors and eruptions of AT 2019krl, M51OT (Jencson et al. 2019), and SN 2008S (Prieto et al. 2008). For SN 2008S we are using the distance derived to NGC 6946 in Anand et al. (2018) of 7.72 Mpc. Right: Hα emission line profiles of SN 2008S type events at around 60–70 days. The AT 2019krl spectrum is from 2019 July 08, the AT 2017be spectrum is unpublished from MMT/Bluechannel taken on 2017 March 08, M51OT is from 2019 March 07 (Jencson et al. 2019), SN 2008S is from 2008 April 25 (Botticella et al. 2009), and SN 2002bu from 2002 June 08 (Smith et al. 2011).

for SN 2008S. It is more ambiguous in the case of AT 2019krl, since a detection was made at the location of the progenitor in the MIPS 24 μm data in 2005, but the mitigating factors of pixel size and the distance of M74 make it difficult to determine if the flux originates from the transient, as opposed to distant surrounding material associated with star formation. If the 24 μm flux comes from AT 2019krl, then it suggests a second region of cooler dust much further out than the warmer dust mapped by the 3.6 μm and 4.5 μm fluxes. Given the uncertain origin of the 24 μm flux and the fact that IRAC data at other MIR wavelengths gave only upper limits, we cannot provide good constraints on a unique fit for this cool component. However, we found that a 60 K blackbody would correspond to a dust ring or shell at radius of 0.2 pc, which is similar to the radii of equatorial rings around other BSGs, as in the inner ring surrounding SN 1987A (Panagia et al. 1991), the ring around Sher25 (Brandner et al. 1997), and the dusty ring around SBW1 (Smith et al. 2007, 2013).

After the discovery of SN 2008S and NGC 300-OT, Thompson et al. (2009) suggested that they constitute a new class of transients that may be caused by ecSNe, an explanation also suggested by Botticella et al. (2009). The explosion of a super-AGB (sAGB) star as an ecSN has an expected kinetic energy of $\sim 10^{50}$ erg, and progenitors are thought to be in the initial mass range 8–10 $M_\odot$. The exact mass range is still debated, and may be very narrow (Doherty et al. 2015). The progenitor photometry for AT 2019krl points to a star more massive than 13 $M_\odot$, and much hotter than an sAGB star. This clearly rules out an ecSN from a sAGB star for the case of AT 2019krl. Additionally, sAGB stars pulsate with large variability ($>$ 1 mag) in their light curves, particularly in the IR (Thompson et al. 2009). These variations are not seen in the progenitor of AT 2019krl (Figure 10), at least to brightness levels that would be above the detection limit of the available *Spitzer* observations.

Plausible alternative progenitor scenarios to this class of events are the outburst of a heavily obscured LBV (Smith et al. 2009, 2011), or other dust enshrouded massive star in a binary system (Berger et al. 2009; Bond et al. 2009; Smith et al. 2011). SN 2008S had an estimated total extinction of $A_V = 2.5$ mag at peak (Prieto et al. 2008) and M51-OT a total reddening $0.7 < E(B-V)[\mathrm{mag}] < 0.9$ (Jencson et al. 2019), which for $R_V = 3.1$ translates to $2.2 < A_V < 2.8$ mag. If we assume a total $A_V = 2.5$ mag for AT 2019krl, then the best fit implies a stellar mass as high as 58 $M_\odot$ from the 2005 *HST* data, or 29.5 $M_\odot$ from the 2013 *HST* data, as we show in Figure 7[9]. Even with lower amounts of extinction, $1.5 < A_V < 2.0$ mag, AT 2019krl would have a

[9] Please note that these mass estimates are made with respect to evolutionary models of single stars that do not include eruptive events and should be interpreted with caution. We therefore do not expect that these accurately reflect the true initial mass of AT 2019krl or its actual evolutionary state, and it should not be surprising that observations at different epochs during an eruption may yield different mass estimates. These are only meant to illustrate the equivalent mass of a single star that might have the same luminosity.

value safely within the expected masses of LBVs (Smith et al. 2004, 2019).

5.3. *Comparison to mergers*

Often referred to as red novae or LRNe, low-mass or intermediate-mass merger candidates can span a wide range of peak magnitudes and progenitor masses, yet may show a similar set of observational signatures (Kochanek et al. 2014; Pastorello et al. 2019). Merger candidates typically exhibit an initial peak in their optical light curve, followed by a secondary peak at some later date. Early-time spectra exhibit a blue continuum with narrow (100–300 km s^{-1}) Balmer emission which fades with time as the spectra redden and cool, until finally molecular absorption lines appear and dominate the spectra a few months after maximum brightness.

In Figure 9 we compare the light curve of AT 2019krl to those of the merger candidates M101-OT (Blagorodnova et al. 2017) and SNHunt248 (Kankare et al. 2015; Mauerhan et al. 2015, 2018). It is still unclear what mechanism is responsible for the multiple light-curve peaks; however, options include a common envelope (CE) ejection for the first peak and a second peak created during the final binary merger, or the first peak being caused by the adiabatic cooling of a CE event, while the second is from CSM interaction with the mass loss during inspiral (Metzger & Pejcha 2017). In the second scenario, viewing angle can easily change the observational signatures of the mergers.

It is possible that AT 2019krl had a double-peaked light curve missed by our sparse post-eruption observations. If so, the overall shape of the light curve fits those of merger candidates, with an absolute luminosity of the progenitor and the outburst being consistent with the class. In particular, the color and temperature of AT 2019krl is quite similar to that of M101 OT2015-1, which was likely a YSG with $T_{\rm eff}$ = 7000 K (Blagorodnova et al. 2017). The progenitor mass and luminosity was quite a bit higher (18 $M_\odot$ and $\log(L/L_\odot) = 4.9$) for the M101 transient, but by adopting a moderately larger extinction, AT 2019krl could have a similar mass (Figure 7). Of course, additional luminosity may come from the inspiral itself; therefore, the mass of the progenitor would be overestimated.

Another obvious discrepancy between AT 2019krl and these merger candidates arises in the spectroscopic evolution. The Hα emission is present and strong at all times in AT 2019krl, while in merger candidates it often fades after peak and may reemerge at late times. LRNe also lack the Ca II NIR and [Ca II] emission that we see in AT 2019krl. Most notably, the molecular bands that form in merger spectra after $\sim$ 100 days are not

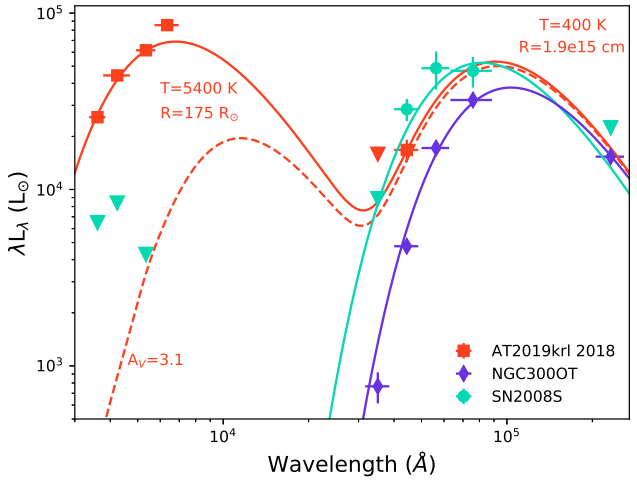

Figure 11. SED of the progenitor of AT 2019krl compared to the progenitors of SN 2008S (Prieto et al. 2008) and NGC 300-OT (Prieto et al. 2009). The MIR of AT 2019krl has been fit assuming a 400 K blackbody as described in the text. The dashed red line shows the combined blackbody fit to the AT 2019krl data (solid line) that has been reddened with $E(B-V) = 1.0$ mag.

seen in AT 2019krl. The lack of molecular lines is not unexpected, as our last photometric observation in 2019 December shows a transient with a temperature of at least 5250 K, still too warm for the creation of molecular lines. It is possible that if the object continues to cool the molecular bands will begin to appear. Only very late-time NIR observations could allow us to detect them.

A complication is that, in principle, mergers can occur across a wide range of initial masses, and mergers in more massive stars might not look the same as lower-mass mergers. For example, in the case of SNHunt248, which had an estimated 60 $M_\odot$ progenitor, no molecular lines were observed in the spectra, and the temperature of the remnant star was estimated to be $T_{\rm eff}$ = 15,000 K (Mauerhan et al. 2018). NGC 4490-OT, another merger candidate, had an estimated mass of 30 $M_\odot$ and strong Hα emission, but the visual-wavelength spectrum closely resembled that of the merger candidate V838 Mon at certain phases (Smith et al. 2016b). Moreover, some individual LBV giant eruptions, including the prototypical case of η Car, have been proposed as massive-star merger events (Smith et al. 2018), and mergers and mass gainers have been invoked to explain evolutionary considerations for LBVs more generally (Justham et al. 2014; Smith & Tombleson 2015; Aghakhanloo et al. 2017). Therefore, the distinction between LBVs and low-mass merger events, such as V1309 Sco and LRNe, might arise simply from a continuum of different initial

masses (Smith et al. 2016b), rather than distinctly different mechanisms.

6. CONCLUSIONS

AT 2019krl shows the observational hallmarks of SN 2008S-type events, which in turn overlap with many observed properties of LBV eruptions. Strong Hα, [Ca II], and Ca II NIR emission are present in its spectra, and the estimated peak absolute magnitude of AT 2019krl is consistent with observed examples of both SN 2008S-like objects and LBV eruptions. The most interesting and significant result of our investigation, however, is the clear evidence that AT 2019krl had a luminous and blue progenitor observed for over 16 yr prior to outburst, as seen in archival *HST* and LBT images, unlike prior SN 2008S-type events. The estimated mass of the progenitor without any local extinction places the star in a mass regime of at least ~ 13 M$_\odot$, although this is a lower limit — a modest increase in the adopted extinction correction could easily move the progenitor to higher masses.

AT 2019krl seems most consistent with a SN2008S-like transient that occurred when a BSG progenitor erupted in a dense disk or toroidal CSM that was observed nearly pole-on. This scenario could arise from binary interaction and a high-mass merger that resembled an LBV outburst. A high-mass BSG progenitor is at odds with the sAGB and ecSN scenario proposed for SN 2008S-like transient events, particularly in cases where it appears that the event is terminal (Adams et al. 2016). Instead, AT 2019krl's BSG progenitor would seem to support earlier interpretations of SN 2008S as an eruption from a dust-obscured BSG star (Smith et al. 2009; Berger et al. 2009; Bond et al. 2009). Deep UV-to-NIR late-time observations with very large ground-based telescopes, *HST*, or *JWST* will allow us to determine if indeed we have a hot luminous star cloaked in a massive dust shell created during the eruption, and if there is both a terminal and nonterminal eruption scenario that can create a very similar transient event.

J.E.A. and N.S. receive support from National Science Foundation (NSF) grant AST-1515559. Research by D.J.S. is supported by NSF grants AST-1821967, 182197, 1813708, 1813466, and 1908972, as well as by the Heising-Simons Foundation under grant #2020-1864. Research by S.V. is supported by NSF grant AST-1813176. K.K. gratefully acknowledges funding from the Deutsche Forschungsgemeinschaft (DFG, German Research Foundation) in the form of an Emmy Noether Research Group (grant number KR4598/2-1). T.S. is supported by the Jnos Bolyai Research Scholarship of the Hungarian Academy of Sciences and by the GINOP-2-3-2-15-2016-00033 project (Transient Astrophysical Objects) of the National Research, Development and Innovation Office (NKFIH), Hungary, funded by the European Union. A.V.F. received funding from NASA/*HST* grants GO-14668, GO-15166, and AR-14295 from the Space Telescope Science Institute (STScI), as well as from the TABASGO Foundation, the Christopher J. Redlich Fund, and the Miller Institute for Basic Research in Science (U.C. Berkeley). Support for *HST* program GO-15151 was provided by NASA through a grant from STScI.

Some of the data reported herein were obtained at the MMT Observatory, a joint facility of the University of Arizona and the Smithsonian Institution. Research at Lick Observatory is partially supported by a generous gift from Google. Based in part on observations made with the NASA/ESA *Hubble Space Telescope*, obtained from the Mikulski Archive for Space Telescopes (MAST) at STScI. STScI is operated by the Association of Universities for Research in Astronomy, Inc. under NASA contract NAS 5-26555. Support for MAST for non-*HST* data is provided by the NASA Office of Space Science via grant NNX13AC07G and by other grants and contracts. This work is based in part on archival data obtained with the *Spitzer Space Telescope*, which is operated by the Jet Propulsion Laboratory, California Institute of Technology, under a contract with NASA. Based in part on observations obtained at the Southern Astrophysical Research (SOAR) telescope, which is a joint project of the Ministério da Ciência, Tecnologia, Inovações e Comunicações (MCTIC) do Brasil, the U.S. National Optical Astronomy Observatory (NOAO), the University of North Carolina at Chapel Hill (UNC), and Michigan State University (MSU). Based in part on observations collected at the European Organisation for Astronomical Research in the Southern Hemisphere under ESO programme ID 098.C-0484(A).

The LBT is an international collaboration among institutions in the United States, Italy, and Germany. LBT Corporation partners are The University of Arizona on behalf of the Arizona university system; Istituto Nazionale di Astrofisica, Italy; LBT Beteiligungsgesellschaft, Germany, representing the Max-Planck Society, the Astrophysical Institute Potsdam, and Heidelberg University; The Ohio State University, and The Research Corporation, on behalf of The University of Notre Dame, University of Minnesota and University of Virginia. Some of the data presented herein were obtained at the W. M. Keck Observatory, which is operated as a scientific partnership among the California Institute of Technology, the University of California, and NASA;

the Observatory was made possible by the generous financial support of the W. M. Keck Foundation. The authors wish to recognize and acknowledge the very significant cultural role and reverence that the summit of Maunakea has always had within the indigenous Hawaiian community. We are most fortunate to have the opportunity to conduct observations from this mountain.

Facilities: HST(ACS,WFC3,WFPC2), SST(IRAC), MMT(Binospec,BCH), LBT(MODS,LBC), Keck(Deimos), SOAR(Goodman)

Software: astropy (Astropy Collaboration et al. 2013),

REFERENCES

Adams, S. M., Kochanek, C. S., Gerke, J. R., & Stanek, K. Z. 2017, MNRAS, 469, 1445

Adams, S. M., Kochanek, C. S., Prieto, J. L., et al. 2016, MNRAS, 460, 1645

Aghakhanloo, M., Murphy, J. W., Smith, N., & Hložek, R. 2017, MNRAS, 472, 591

Ahn, C. P., Alexandroff, R., Allende Prieto, C., et al. 2012, ApJS, 203, 21

Alard, C. 2000, A&AS, 144, 363

Alard, C., & Lupton, R. H. 1998, ApJ, 503, 325

Anand, G. S., Rizzi, L., & Tully, R. B. 2018, AJ, 156, 105

Andrews, J., Sand, D., Smith, N., et al. 2019, The Astronomer's Telegram, 12913, 1

Aret, A., Kraus, M., & Šlechta, M. 2016, MNRAS, 456, 1424

Asplund, M., Grevesse, N., Sauval, A. J., & Scott, P. 2009, ARA&A, 47, 481

Astropy Collaboration, Robitaille, T. P., Tollerud, E. J., et al. 2013, A&A, 558, A33

Bacon, R., Accardo, M., Adjali, L., et al. 2010, in Society of Photo-Optical Instrumentation Engineers (SPIE) Conference Series, Vol. 7735, Ground-based and Airborne Instrumentation for Astronomy III, 773508

Beasor, E. R., & Davies, B. 2018, MNRAS, 475, 55

Bellm, E. C., Kulkarni, S. R., Graham, M. J., et al. 2019, PASP, 131, 018002

Berg, D. A., Skillman, E. D., Croxall, K. V., et al. 2015, ApJ, 806, 16

Berger, E., Soderberg, A. M., Chevalier, R. A., et al. 2009, ApJ, 699, 1850

Blagorodnova, N., Kotak, R., Polshaw, J., et al. 2017, ApJ, 834, 107

Blagorodnova, N., Karambelkar, V., Adams, S. M., et al. 2020, MNRAS, 496, 5503

Bond, H. E., Bedin, L. R., Bonanos, A. Z., et al. 2009, ApJL, 695, L154

Bond, H. E., Henden, A., Levay, Z. G., et al. 2003, Nature, 422, 405

Botticella, M. T., Pastorello, A., Smartt, S. J., et al. 2009, MNRAS, 398, 1041

Brandner, W., Chu, Y.-H., Eisenhauer, F., Grebel, E. K., & Points, S. D. 1997, ApJL, 489, L153

Bruzual, G., & Charlot, S. 2003, MNRAS, 344, 1000

Cai, Y. Z., Pastorello, A., Fraser, M., et al. 2018, MNRAS, 480, 3424

Calzetti, D., Armus, L., Bohlin, R. C., et al. 2000, ApJ, 533, 682

Cappellari, M. 2017, MNRAS, 466, 798

Cappellari, M., & Emsellem, E. 2004, PASP, 116, 138

Castelli, F., & Kurucz, R. L. 2003, in IAU Symposium, Vol. 210, Modelling of Stellar Atmospheres, ed. N. Piskunov, W. W. Weiss, & D. F. Gray, A20

Choi, J., Dotter, A., Conroy, C., et al. 2016, ApJ, 823, 102

Clemens, J. C., Crain, J. A., & Anderson, R. 2004, in Society of Photo-Optical Instrumentation Engineers (SPIE) Conference Series, Vol. 5492, Ground-based Instrumentation for Astronomy, ed. A. F. M. Moorwood & M. Iye, 331–340

de Jaeger, T., Anderson, J. P., Galbany, L., et al. 2018, MNRAS, 476, 4592

Doherty, C. L., Gil-Pons, P., Siess, L., Lattanzio, J. C., & Lau, H. H. B. 2015, MNRAS, 446, 2599

Dolphin, A. 2016, DOLPHOT: Stellar photometry, , , ascl:1608.013

Dolphin, A. E. 2000, PASP, 112, 1383

Dong, S., Kochanek, C. S., Adams, S., & Prieto, J. L. 2015, The Astronomer's Telegram, 7173, 1

Dotter, A. 2016, ApJS, 222, 8

Drout, M. R., Soderberg, A. M., Gal-Yam, A., et al. 2011, ApJ, 741, 97

Faber, S. M., Phillips, A. C., Kibrick, R. I., et al. 2003, in Society of Photo-Optical Instrumentation Engineers (SPIE) Conference Series, Vol. 4841, Instrument Design and Performance for Optical/Infrared Ground-based Telescopes, ed. M. Iye & A. F. M. Moorwood, 1657–1669

Fabricant, D., Fata, R., Epps, H., et al. 2019, PASP, 131, 075004

Fazio, G. G., Hora, J. L., Allen, L. E., et al. 2004, ApJS, 154, 10

Filippenko, A. V. 1982, PASP, 94, 715

Foley, R. J., Berger, E., Fox, O., et al. 2011, ApJ, 732, 32
Gaia Collaboration, Brown, A. G. A., Vallenari, A., et al. 2018, A&A, 616, A1
Gehrz, R. D., Roellig, T. L., Werner, M. W., et al. 2007, Review of Scientific Instruments, 78, 011302
Gerke, J. R., Kochanek, C. S., & Stanek, K. Z. 2015, MNRAS, 450, 3289
Giallongo, E., Ragazzoni, R., Grazian, A., et al. 2008, A&A, 482, 349
Goldman, S. R., van Loon, J. T., Zijlstra, A. A., et al. 2017, MNRAS, 465, 403
Goranskij, V. P., Barsukova, E. A., Spiridonova, O. I., et al. 2016, Astrophysical Bulletin, 71, 82
Hack, W. J., Dencheva, N., Fruchter, A. S., et al. 2012, in American Astronomical Society Meeting Abstracts, Vol. 220, American Astronomical Society Meeting Abstracts #220, 135.15
Ho, A. 2019, Transient Name Server Discovery Report, 2019-1165, 1
Humphreys, R. M., Bond, H. E., Bedin, L. R., et al. 2011, ApJ, 743, 118
Humphreys, R. M., Davidson, K., & Smith, N. 1999, PASP, 111, 1124
Jencson, J. E., Adams, S. M., Bond, H. E., et al. 2019, ApJL, 880, L20
Jordi, K., Grebel, E. K., & Ammon, K. 2006, A&A, 460, 339
Justham, S., Podsiadlowski, P., & Vink, J. S. 2014, ApJ, 796, 121
Kankare, E., Kotak, R., Pastorello, A., et al. 2015, A&A, 581, L4
Kansky, J., Chilingarian, I., Fabricant, D., et al. 2019, PASP, 131, 075005
Kasliwal, M. M., Kulkarni, S. R., Arcavi, I., et al. 2011, ApJ, 730, 134
Kasliwal, M. M., Bally, J., Masci, F., et al. 2017, ApJ, 839, 88
Kennicutt, Robert C., J., Armus, L., Bendo, G., et al. 2003, PASP, 115, 928
Kochanek, C. S. 2011, ApJ, 743, 73
Kochanek, C. S., Adams, S. M., & Belczynski, K. 2014, MNRAS, 443, 1319
Kochanek, C. S., Beacom, J. F., Kistler, M. D., et al. 2008, ApJ, 684, 1336
Kochanek, C. S., Szczygieł, D. M., & Stanek, K. Z. 2012, ApJ, 758, 142
Kreckel, K., Groves, B., Bigiel, F., et al. 2017, ApJ, 834, 174
Kreckel, K., Groves, B., Schinnerer, E., et al. 2013, ApJ, 771, 62
Kreckel, K., Faesi, C., Kruijssen, J. M. D., et al. 2018, ApJL, 863, L21
Kreckel, K., Ho, I. T., Blanc, G. A., et al. 2019, ApJ, 887, 80
MacLeod, M., Macias, P., Ramirez-Ruiz, E., et al. 2017, ApJ, 835, 282
Mason, E., Diaz, M., Williams, R. E., Preston, G., & Bensby, T. 2010, A&A, 516, A108
Mauerhan, J. C., Van Dyk, S. D., Johansson, J., et al. 2018, MNRAS, 473, 3765
Mauerhan, J. C., Van Dyk, S. D., Graham, M. L., et al. 2015, MNRAS, 447, 1922
Mauron, N., & Josselin, E. 2011, A&A, 526, A156
McQuinn, K. B. W., Skillman, E. D., Dolphin, A. E., Berg, D., & Kennicutt, R. 2017, AJ, 154, 51
Metzger, B. D., & Pejcha, O. 2017, MNRAS, 471, 3200
Ohsawa, R., Sakon, I., Onaka, T., et al. 2010, ApJ, 718, 1456
Owocki, S. P., Gayley, K. G., & Shaviv, N. J. 2004, ApJ, 616, 525
Panagia, N., Gilmozzi, R., Macchetto, F., Adorf, H. M., & Kirshner, R. P. 1991, ApJL, 380, L23
Pastorello, A., Mason, E., Taubenberger, S., et al. 2019, A&A, 630, A75
Patat, F., Maund, J. R., Benetti, S., et al. 2010, A&A, 510, A108
Pejcha, O. 2014, ApJ, 788, 22
Phillips, M. M., Simon, J. D., Morrell, N., et al. 2013, ApJ, 779, 38
Pogge, R. W., Atwood, B., Brewer, D. F., et al. 2010, in Society of Photo-Optical Instrumentation Engineers (SPIE) Conference Series, Vol. 7735, Ground-based and Airborne Instrumentation for Astronomy III, 77350A
Poznanski, D., Prochaska, J. X., & Bloom, J. S. 2012, MNRAS, 426, 1465
Prieto, J. L., Sellgren, K., Thompson, T. A., & Kochanek, C. S. 2009, ApJ, 705, 1425
Prieto, J. L., Kistler, M. D., Thompson, T. A., et al. 2008, ApJL, 681, L9
Prieto, J. L., Rest, A., Bianco, F. B., et al. 2014, ApJL, 787, L8
Schlafly, E. F., & Finkbeiner, D. P. 2011, ApJ, 737, 103
Shiode, J. H., & Quataert, E. 2014, ApJ, 780, 96
Smith, N. 2012, Astrophysics and Space Science Library, Vol. 384, All Things Homunculus, ed. K. Davidson & R. M. Humphreys, 145
Smith, N., Aghakhanloo, M., Murphy, J. W., et al. 2019, MNRAS, 488, 1760
Smith, N., Andrews, J. E., Mauerhan, J. C., et al. 2016a, MNRAS, 455, 3546

Smith, N., & Arnett, W. D. 2014, ApJ, 785, 82
Smith, N., Arnett, W. D., Bally, J., Ginsburg, A., & Filippenko, A. V. 2013, MNRAS, 429, 1324
Smith, N., Bally, J., & Walawender, J. 2007, AJ, 134, 846
Smith, N., & Frew, D. J. 2011, MNRAS, 415, 2009
Smith, N., Gehrz, R. D., Stahl, O., Balick, B., & Kaufer, A. 2002, ApJ, 578, 464
Smith, N., Li, W., Silverman, J. M., Ganeshalingam, M., & Filippenko, A. V. 2011, MNRAS, 415, 773
Smith, N., & Morse, J. A. 2004, ApJ, 605, 854
Smith, N., & Owocki, S. P. 2006, ApJL, 645, L45
Smith, N., & Tombleson, R. 2015, MNRAS, 447, 598
Smith, N., Vink, J. S., & de Koter, A. 2004, ApJ, 615, 475
Smith, N., Ganeshalingam, M., Chornock, R., et al. 2009, ApJL, 697, L49
Smith, N., Miller, A., Li, W., et al. 2010, AJ, 139, 1451
Smith, N., Andrews, J. E., Van Dyk, S. D., et al. 2016b, MNRAS, 458, 950
Smith, N., Andrews, J. E., Rest, A., et al. 2018, MNRAS, 480, 1466
Soker, N., & Kashi, A. 2013, ApJL, 764, L6
Sparks, W. B., Bond, H. E., Cracraft, M., et al. 2008, AJ, 135, 605
Stritzinger, M. D., Taddia, F., Burns, C. R., et al. 2018, A&A, 609, A135
Szalai, T., Fox, O. D., Marston, T., et al. 2019, The Astronomer's Telegram, 12934, 1
Szczygieł, D. M., Kochanek, C. S., & Dai, X. 2012, ApJ, 760, 20
Tammann, G. A., & Sandage, A. 1968, ApJ, 151, 825
Thompson, T. A., Prieto, J. L., Stanek, K. Z., et al. 2009, ApJ, 705, 1364
Tylenda, R., Hajduk, M., Kamiński, T., et al. 2011, A&A, 528, A114
Van Dyk, S. D., Filippenko, A. V., Chornock, R., Li, W., & Challis, P. M. 2005, PASP, 117, 553
Van Dyk, S. D., & Matheson, T. 2012, Astrophysics and Space Science Library, Vol. 384, The Supernova Impostors, ed. K. Davidson & R. M. Humphreys, 249
Van Dyk, S. D., Peng, C. Y., King, J. Y., et al. 2000, PASP, 112, 1532
Weilbacher, P. M., Palsa, R., Streicher, O., et al. 2020, A&A, 641, A28
Werner, M. W., Roellig, T. L., Low, F. J., et al. 2004, ApJS, 154, 1
Williams, S. C., Jones, D., Pessev, P., et al. 2020, A&A, 637, A20